Numerical study on acoustic oscillations of 2D and 3D flue organ pipe like instruments with compressible LES

Masataka MIYAMOTO, Yasunori ITO, Takuya IWASAKI, Takahiro AKAMURA, Kin'ya TAKAHASHI,
The Physics Laboratories, Kyushu Institute of Technology, Kawazu 680-4, Iizuka 820-8502, Japan

Toshiya TAKAMI, Taizo KOBAYASHI, Akira NISHIDA, Mutsumi AOYAGI
Research Institute for Information Technology, Kyushu University,
6-10-1 Hakozaki, Higashi-ku, Fukuoka 812-8581, Japan

April 30, 2012

Abstract

Acoustic oscillations of flue instruments are investigated numerically using compressible Large Eddy Simulation (LES). Investigating 2D and 3D models of flue instruments, we reproduce acoustic oscillations excited in the resonators as well as an important characteristic feature of flue instruments – the relation between the acoustic frequency and the jet velocity described by the semi-empirical theory developed by Cremer & Ising, Coltman and Fletcher *et al.* based on experimental results. Both 2D and 3D models exhibit almost the same oscillation frequency for a given jet velocity, but the acoustic oscillation as well as the jet motion is more stable in the 3D model than in the 2D model, due to less stability in 3D fluid of the rolled up eddies created by the collision of the jet with the edge, which largely disturb the jet motion and acoustic field in the 2D model. We also investigate the ratio of the amplitude of the acoustic flow through the mouth opening to the jet velocity, comparing with the experimental results and semi-empirical theory given by Hirschberg *et al.*.

PACS numbers: 43.75.Qr,43.75.Np,43.75.Ef,43.75.-z,43.28.Ra

1 Introduction

The acoustical mechanism of flue instruments is a long standing problem in the field of musical acoustics and it is still not understood completely[1, 2, 3]. The sound source of flue instruments is an aerodynamic sound source, a so-called edge tone, which is generated by an oscillating air jet colliding with an edge[4, 5, 6]. The major difficulty in analyzing the acoustic mechanism of flue instruments is the strong and complex interactions between the air flow dynamics acting as the sound source and the acoustic field excited by it in the resonator [1, 2, 3, 6]. Indeed, the acoustic pressure in the resonance pipe exceeds 140dB and it compels the jet motion to synchronize with it. In order to elucidate this mechanism in detail, we need to study the dynamics of the jet flow in terms of fluid dynamics as well as that of the acoustic field in terms of acoustics, at the same time taking into account the complex interaction between them. From the numerical point of view, this requires simultaneous reproduction of fluid dynamics and acoustic field by a compressible fluid solver. However, the method to treat this problem has not been established yet.

In the long history of study of the edge tone, some phenomenological formulas which describe the relation between the edge tone frequency and the jet velocity have been proposed [4, 5, 6, 7, 8]. A very useful formula introduced by Brown[4] based on experimental results shows that the frequency linearly increases with the jet velocity. In the field of musical acoustics, a phenomenological theory that describes the behavior of flue instruments has been developed since 1960's[1, 3]. The mechanism by which the air jet drives the resonator was studied by several authors experimentally and theoretically, chief pioneers being Cremer and Ising, and Coltman[9, 10, 11, 12, 13, 14, 15, 16, 17, 18, 19, 20, 21]. Theory that describes the behavior of the resonator driven by the air jet has also been developed with the help of equivalent electrical circuit theory[9, 10, 11, 12, 13, 14, 15, 16, 17, 18]. As a result, the difference in oscillations between the pure edge tone and the flue instrument has been clarified in regard to the relation between the acoustic frequency and the jet velocity[1, 13].

However, the theory developed in the field of musical acoustics includes many conceptual approximations and is far from rigorous. A rigorous theory must be based upon the Navier-Stokes equations of fluid dynamics, and include the role of the vorticity field of a real fluid as a sound source in complex geometry of instruments. The aerodynamic sound source was first formulated by Lighthill [22]. Lighthill introduced an inhomogeneous wave equation whose inhomogeneous term behaves as a quadrupole source term, the so-called Lighthill's acoustic analogy. Lighthill's analogy well predicts the aerodynamic sound from the localized turbulence in free space. Curle improved Lighthill's analogy in order to treat the case of arbitrary boundary condition by using Green's formula: the boundary effect is estimated by a surface integral, which behaves like dipole sources and usually dominates the quadrupole sources in a low Mach regime[23, 24]. Powell and Howe followed Lighthill's work and introduced a very important notion that the major part of Lighthill's sources comes from unsteady motion of vortices, namely vortex sound [25, 26]. Howe also introduced a formula, known as Howe's energy corollary, which allows estimation of the energy transfer between the hydrodynamic field and the acoustic field caused by the non-linear interaction between them[27].

Further, Howe discussed the acoustic mechanism of flue instruments in terms of the vortex sound theory [6, 26]. Based on the jet-drive model introduced by Powell and Coltman[5, 13] and taking into account Howe's energy corollary and some other hydrodynamic theories, Hirschberg and his coworkers introduced a global source model combined with the acoustical energy losses due to vortex-shedding at the labium [2, 3, 28, 29, 30, 31, 32, 33]. This model allows estimation of the ratio of the amplitude of the acoustic flow through the mouth opening to the jet velocity related with the geometry of the mouth opening.

Recently, several authors have tried to numerically reproduce the acoustic oscillations of edge tones and those of flue instruments by using fluid solvers, e.g., FEM, Lattice-Boltzmann-Method (LBM), Large Eddy Simulation (LES) and so on, and have got some important results [34, 35, 36, 37, 38, 39, 40, 41, 42, 43, 44, 45]. There also have been experimental and theoretical reports of

importance [3, 46, 47, 48, 49, 50, 51, 52, 53, 54]. Nevertheless, the detailed mechanisms of sound production by the air jet and of jet-resonator interaction are still not completely understood.

The final goal of our study is to analyze the interaction of the jet flow with the acoustic field excited in the resonator and to explain the sound production mechanism of flue instruments in terms of the theory of aerodynamic sound. In previous works [39, 40, 41, 42], first we numerically calculated 2D and 3D edge tone models by using a compressible fluid solver, the compressible LES (Large Eddy Simulation) [55], and demonstrated that both 2D and 3D models well reproduce the Brown equation though the 3D model is in better agreement [40]. Next, we numerically reproduced acoustic oscillations in a 2D model of a small recorder type flue instrument with an open end [41, 42], and reported that the model well captures the characteristic feature of flue instruments – the relation between the acoustic frequency and the jet velocity described by the semi-empirical theory developed by Cremer & Ising, Coltman and Fletcher *et al.*[9, 10, 11, 12, 13, 14, 15, 16, 17, 18]. Further, in a preliminary calculation, we reproduced an acoustic oscillation of a 3D ocarina model, though it was done for a short time interval [39].

In this paper, we numerically study acoustic oscillations in 2D and 3D models of a small flue instrument with a closed end. Our 3D model is a quasi-2D model consisting of a volume between two parallel non-slip walls, due to the limitation of computation power. However, it is very similar in the geometry near the mouth opening to that experimentally studied by Coltman[13]. Due to a weaker reflectance at the 2D open end compared with that at the 3D open end, oscillations in the pipe with a closed end are more stable than those in the pipe with an open end. So we choose models with a closed end in this paper. Specifically, we numerically produce time evolutions of pressure, velocity, vorticity, and Lighthill's source distributions inside and outside the 2D and 3D instruments by compressible LES. Although differences between 2D and 3D models observed using LBM were briefly reported by Kühnelt[36, 37], we clarify crucial differences between 2D and 3D models in fluid dynamics and acoustics. We also investigate the relation between the acoustic frequency and the jet velocity in detail, comparing with the semi-empirical theory developed by Cremer & Ising, Coltman and Fletcher *et al.* [9, 10, 11, 12, 13, 14, 15, 16, 17, 18]. Further, we investigate the ratio of the amplitude of the acoustic flow through the mouth opening to the jet velocity, comparing with the experimental results and semi-empirical theory given by Hirschberg *et al.*[2, 3, 28, 29, 30, 31, 32, 33].

The organization of the present paper is as follows. In section 2, we review previous studies related to the sound production of flue instruments. We briefly explain Lighthill's theory, Curle's extension, Howe's energy corollary and Brown's work on the edge tone. Further, we explain the phenomenological theory of flue instruments developed by Cremer & Ising, Coltman and Fletcher *et al.* and its drawbacks. An alternative method introduced by Hirschberg *et al.* is briefly introduced. In section 3, we introduce our model instruments, 2D and 3D small flue instruments with a closed end, and explain the environment of numerical calculations. In section 4, we show the results of the numerical analysis. First we compare the 3D model with the 2D model at an optimal choice of jet velocity at which the most stable acoustic oscillation is observed for the 2D model. The 2D and 3D models have almost the same oscillation frequency, but the 3D model is more stable in acoustic oscillation as well as in jet motion than the 2D model, due to less stability in 3D fluid of rolled up eddies which disturb the jet motion and acoustic field. We also study the change of acoustic frequency with increase of the jet velocity, mainly using 2D results, comparing with the prediction given by the phenomenological theory of flue instruments introduced in section 2. Finally, we investigate the energy transfer rate from hydrodynamic energy to acoustic energy in the 2D and quasi-2D models, comparing with results of real 3D instruments reported in refs.[3, 29, 30, 31, 32, 33]. Section 5 is devoted to a summary and discussion. In Appendix, we develop the theory of radiation impedance at a 2D flanged pipe and compare it with the 3D theory.

2 Theory related to sound production of flue instruments

2.1 Lighthill's Theory

The sound generated by subsonic unsteady flows is usually called aerodynamic sound, which is a very small byproduct of the motion of unsteady flows of high Reynolds numbers. The source of aerodynamic sound was first formulated by Lighthill[22]. Lighthill transformed exactly the set of fundamental equations, Navier-Stokes and continuity equations, to an inhomogeneous wave equation whose inhomogeneous term plays the role of the source:

$$\left(\frac{\partial^2}{\partial t^2} - c_0^2\nabla^2\right)(\rho-\rho_0) = \frac{\partial^2 T_{ij}}{\partial x_i \partial x_j}, \tag{1}$$

where the tensor T_{ij} is called Lighthill's tensor and is defined by

$$T_{ij} = \rho v_i v_j + ((p-p_0) - c_0^2(\rho-\rho_0))\delta_{ij} + \sigma_{ij}. \tag{2}$$

Here, c_0 denotes the speed of sound in equilibrium air, p the air pressure, p_0 the average air pressure (i.e. equilibrium pressure), ρ the air density, ρ_0 the average air density (i.e. equilibrium air density), and σ_{ij} the viscous stress tensor. The sound is generated by the localized turbulence(or unsteady flows), namely the quadrupole source distribution given by the inhomogeneous term in RHS of eq.(1), and it is regarded as a wave propagating in a stationary acoustic medium. This is Lighthill's acoustic analogy.

Since the dissipation by σ_{ij} can be ignored for high Reynolds numbers and adiabaticity is well maintained with $(p-p_0) - c_0^2(\rho-\rho_0) = 0$, then the first term of eq.(2), $\rho v_i v_j$, becomes the major term of the source. Further, particle velocities of the sound are usually sufficiently small compared with those of the real flow that the source term is well approximated by that obtained from an incompressible fluid with $\rho = \rho_0$ and div $v = 0$. Even for the case that a strong acoustic field exists, that is, the acoustically induced particle velocities in the mouth opening can reach 30% of the jet flow velocity V for organ pipes[30, 31, 32, 33], the acoustic flow can be safely assumed to be locally incompressible, if the flow is of low Mach number($V/c_0 \ll 1$) and of low Helmholtz number($fh/c_0 \ll 1$), where f and h denote the frequency of acoustic oscillation and the height of the pipe, respectively. Then the incompressible fluid approximation is also applicable. Note that we use the definition of the acoustic flow as the unsteady component part of the flow defined by a scalar potential or, with almost the same meaning, as the time dependent compressible component of a scalar potential flow[6, 26, 27]. Then, the sound source is given by

$$\begin{aligned}\frac{\partial^2 T_{ij}}{\partial x_i \partial x_j} &\sim \rho_0 \frac{\partial^2 v_i v_j}{\partial x_i \partial x_j} \\ &= \rho_0(s_{ij}^2 - w_{ij}^2),\end{aligned} \tag{3}$$

where s_{ij} and w_{ij} are respectively given by

$$s_{ij} = \frac{1}{2}\left(\frac{\partial v_j}{\partial x_i} + \frac{\partial v_i}{\partial x_j}\right), \tag{4}$$

$$w_{ij} = \frac{1}{2}\left(\frac{\partial v_j}{\partial x_i} - \frac{\partial v_i}{\partial x_j}\right). \tag{5}$$

For a 2D fluid, it reduces to

$$\frac{\partial^2 T_{ij}}{\partial x_i \partial x_j} \sim -2\rho_0\left(\frac{\partial v_1}{\partial x_1}\frac{\partial v_2}{\partial x_2} - \frac{\partial v_2}{\partial x_1}\frac{\partial v_1}{\partial x_2}\right). \tag{6}$$

In the calculation of Lighthill's sources in section 4, we will use the formula eqs.(3) and (6) for 3D and 2D models, respectively.

Lighthill's analogy well predicts the aerodynamic sound from localized turbulence in free space. However, in the case that solid bodies exist, the quadrupoles $\frac{\partial^2 T_{ij}}{\partial x_i \partial x_j}$ will no longer be distributed over the whole of space, but only throughout the region outside of the solid bodies, and it seems that a resultant distribution of dipoles(or even sources) at the boundaries generated by unsteady force of the walls on the flow usually dominates the quadrupoles. Curle estimated the dipoles on the boundaries in terms of surface integrals by using Green's formula based on Lighthill's equation (1)[23]. However, the surface integrals are usually estimated in terms of the free Green function, i.e., Green function in the free space, so that the integrals include not only the effect of the unsteady force but also the reflection and diffraction of sound at the solid boundaries[23, 24]. In the case that a strong acoustic field exists, as in the resonator of a

musical instrument, it is difficult to separate the true surface force effect from the acoustic reflection and diffraction in the surface integrals. Of course this is formally possible by using the Green function that satisfies the acoustic boundary condition at the solid surfaces under consideration, but it is hard to obtain in practice for arbitrary boundary shapes. So we do not discuss the Curle formula in this paper and will leave it as a future problem.

An alternative way to estimate the energy transfer between the acoustic field and the hydrodynamic field was proposed by Howe[27]. The energy change per unit time Π due to the interaction between the acoustic field and the hydrodynamic field is given by a volume integral, known as Howe's energy corollary:

$$\Pi = \rho_0 \int (\boldsymbol{\omega} \wedge \boldsymbol{v}) \cdot \bar{\boldsymbol{v}} \, \mathrm{d}\boldsymbol{r}, \tag{7}$$

where $\boldsymbol{\omega}$ is the vorticity($\boldsymbol{\omega} = \mathrm{rot}\boldsymbol{v}$) and $\bar{\boldsymbol{v}}$ denotes an acoustic flow. Although this integral is taken over the entire space without any solid boundaries, it is expected that the term $(\boldsymbol{\omega} \wedge \boldsymbol{v}) \cdot \bar{\boldsymbol{v}}$ gives a local energy transfer rate between the acoustic field and the hydrodynamic field. However there is no established method to extract the acoustic flow from the complete velocity field obtained numerically with enough accuracy. So we do not treat Howe's method in this paper. Note that there are some experimental techniques (or hybrid methods combining measurement with numerical calculation) to estimate the acoustic field by using an external driving source, e.g., loud speaker in non-hydrodynamic field[48, 49, 56, 57]. It is also possible to roughly estimate the acoustic flow through the mouth from the data of pressure in the resonator for flue instruments[29, 31].

2.2 Edge tone

As illustrated in Fig.1, the edge tone is an aerodynamic sound generated by the unsteady but mostly periodic oscillation of a jet emanated from a flue and colliding with an edge. The edge tone is the sound source of flue instruments[1, 2, 6]. Although the detailed mechanism of the production of edge tone has not been completely understood yet, its characteristic features have been well captured by semi-empirical equations based on experimental results. One equation was introduced by Brown to predict the edge tone frequency[4]:

$$f = a_1 j(a_2 V - a_3)(1/(a_4 l) - a_5), \tag{8}$$

where V denotes the speed of the jet and l is the distance between the flue and the edge in the SI units. The parameters are taken as $a_1 = 0.446$(dimensionless), $a_2 = 100$(dimensionless), $a_3 = 40$m/s, $a_4 = 100\mathrm{m}^{-2}$ and $a_5 = 0.07$m, where we presume the dimensions of the parameters, because they were not specified in the original paper [4]. The values of number j are taken as $j = 1.0, 2.3, 3.8$ and 5.4. The value $j = 1$ corresponds to the first hydrodynamic mode (or the first Stage [6]) and other values correspond to higher hydrodynamic modes. The frequency of the first mode increases linearly with increase of V. But the oscillation jumps to one of the higher modes if V exceeds a threshold value. The transition is hysteretic, namely the downward transition has a different threshold value. Usually, the first mode is used for flue instruments with a small distance l.

In a preliminary study [40], we confirmed that numerically calculations using a compressible LES solver are in good agreement with Brown's equation at several values of the jet velocity for a 3D model and that even a 2D model agrees well with Brown's equation in a physically important range of the jet velocity. This confirms the validity of calculations with LES for 2D and 3D models of flue instruments in this paper. Note that Brown's equation has also been reproduced using several different numerical schemes, including Finite Element Method(FEM) [38].

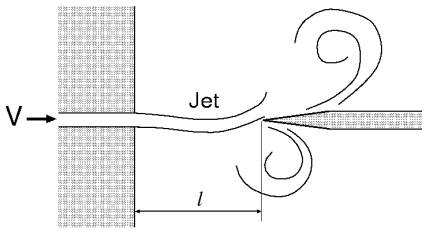

Figure 1: Edge tone.

2.3 Phenomenological theory of flue instruments

The driving mechanism of flue instruments was first studied in the pioneering works of Cremer & Ising, and Coltman [9, 10, 11, 12, 13, 14], which were followed later by many authors [18, 19, 20, 21]. These studies have made clear the differences in driving mechanism between the edge tone and the flue instrument with a resonator. In the following, we describe the outline of the regenerative excitation mechanism of flue instruments according to the text book by Fletcher and Rossing [1].

The jet which emanates from a flue with the velocity V and is disturbed by a uniform transverse acoustic-flow $\bar{v}_y \exp(i\omega t)$ forms an oscillating wave which propagates with a velocity u and grows exponentially with a growth parameter μ. The wave of the jet propagating in x-direction is well approximated by the semi-empirical equation (also see Fig.2), which gives the position in y-direction as a function of x and t:

$$\begin{aligned} J(x,t) &= -i\frac{\bar{v}_y}{\omega}\big\{\exp(i\omega t) \\ &\quad -\cosh(\mu x)\exp(i\omega(t-x/u))\big\}. \end{aligned} \tag{9}$$

Except for the case that $\bar{k}d$ is extremely small, where $\bar{k}$ and d stand for the angular wave number and the height of flue aperture, respectively, we can use approximations $u \approx V/2$ and $\mu \approx \bar{k}$. We always assume these approximations in the following. In this formula, the existence of the edge, which plays an important role in formation of the jet oscillation, is ignored. Thus it should be considered that eq.(9) only gives the lowest order approximation of the jet motion.

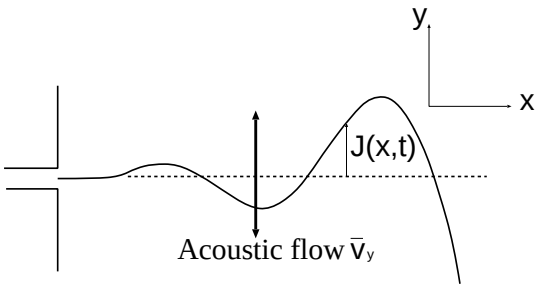

Figure 2: Jet oscillation.

Taking into account the jet oscillation given by eq.(9), we can describe the sound excitation mechanism of flue instruments. To do this, we separate the system into a generator and a resonator by a plane S_p as shown in Fig3(a). Making use of an equivalent circuit network (see Fig.3(b)), we can determine the oscillation condition, which gives acoustic frequencies of the modes as functions of the jet velocity.

The net flow out of the resonator across the plane P is given by

$$U = U_m - U_j. \tag{10}$$

U_m is the acoustic flow out through the mouth of the resonator, which is estimated by

$$U_m \approx \frac{p_m S_p}{i\omega\rho\Delta L_m}. \tag{11}$$

ΔL_m denotes the end correction at the open mouth and $i\omega\rho\Delta L_m/S_p$ is regarded as the mouth impedance, then ΔL_m may be taken as $\Delta L_m \approx 2\Delta L_{2D,3D}$, which is the end correction of the 2D or 3D flanged pipe(see Appendix)[58]. S_p is the cross section at the plane P and the pressure p_m at the mouth is related with the pressure p_p at the plane P as

$$p_p = p_m\left(1 - \frac{V^2 WG}{\omega^2 \Delta L_m S_m}\right) \tag{12}$$

where G is defined by

$$\begin{aligned} G &= \frac{J(l,t)}{i2\bar{v}_y \exp(i\omega t)/\omega} \\ &= \frac{1}{2}\big(\cosh(\mu l)\exp(-i\omega l/u) - 1\big), \end{aligned} \tag{13}$$

W is the width of the jet in its planar transverse direction and an effective cross-section S_m is defined by $S_m \equiv S_p - S_j$, where S_j is a (mean) fraction of cross section of the jet which enters the resonator. U_j is the oscillating part of the jet flow into the resonator, which is estimated by

$$U_j \approx -\frac{VWG}{\rho\omega^2\Delta L_m}\left(\frac{S_p}{S_m}\right)p_m. \tag{14}$$

Then, the total generator admittance is defined by

$$Y_g = U/p_p. \tag{15}$$

As was done in ref.[1], under the assumption that $\cosh(\mu l) \gg 1$ and $\frac{V^2 WG}{\omega^2 \Delta L_m S_m} \ll 1$, Y_g is approximated by

$$Y_g \approx \frac{p_m S_p}{i\omega\rho\Delta L_m} + \frac{VW}{2\rho\omega^2\Delta L_m}\left(1+\frac{V}{i\omega\Delta L_m}\right) \times \left(\frac{S_p}{S_m}\right)\cosh(\mu l)\exp(-i\omega l/u). \quad (16)$$

However, we do not use this approximation in this paper, because the full calculation is more accurate.

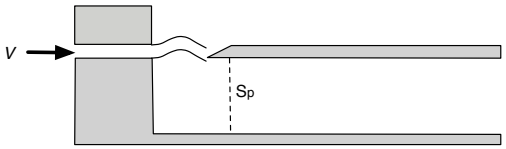

(a) Pipe driven by jet.

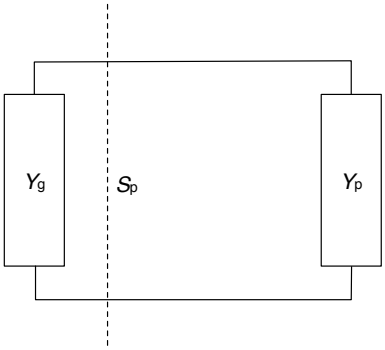

(b) Equivalent circuit network.

Figure 3: Regenerative excitation mechanism.

The stability condition of the network in Fig.3(b) is given by

$$Y_g + Y_p = 0, \quad (17)$$

where the pipe admittance Y_p has the following forms: $Y_p = -i\frac{S_p}{\rho c_0}\cot kL$ for an open end pipe with a length L, and $Y_p = i\frac{S_p}{\rho c_0}\tan kL$ for a closed end pipe. It is convenient to separate the condition (17) into the real and imaginary parts,

$$\mathrm{Re}Y_g < 0, \quad (18)$$

$$\mathrm{Im}(Y_g + Y_p) = 0. \quad (19)$$

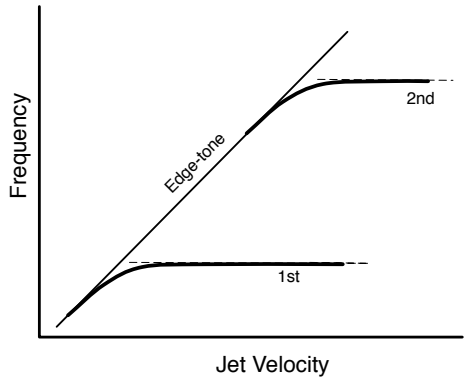

Figure 4: Oscillation frequency vs. jet velocity for a closed end pipe.

Eq.(18) indicates that the generator must have a negative resistance as a power supplier that excites the system, overcoming non-zero resistance of the mouth and pipe. For given pipe geometry, closed or opened end, the imaginary part (19) gives the oscillating condition, that is, it determines the oscillating frequency at a given jet velocity V. For the case of $Y_p = 0$, i.e., without any resonator, eq.(19) should provide the oscillating condition of the edge tone.

Fig.4 schematically illustrates the frequency of the acoustic wave as a function of the jet velocity V given by eq.(19) for the closed end pipe together with the edge tone frequency in eq.(8) with $j = 1$. The frequency of the acoustic wave first increases in proportion to the jet velocity, similarly to the edge tone(the first hydrodynamic mode), but it synchronizes with the first acoustic pipe mode if the edge tone frequency comes near the fundamental frequency. Locking to the fundamental continues until the edge tone frequency is close to the second acoustic pipe mode frequency (the third harmonic for the closed end pipe) and then the frequency of the acoustic wave jumps up to the second resonance. The same process is repeated each time the edge tone frequency reaches the next resonance frequency.

Therefore, the theory introduced above is useful to predict the frequency of acoustic oscillation excited in the pipe, but it has some drawbacks in estimation of the intensity of sound wave in the pipe and the energy loss occurring due to the in-

teraction between the acoustic field and the fluid flow near the mouth opening [12, 30, 31, 32, 33]. Hirschberg and his coworkers pursued this problem in semi-empirical ways [3, 28, 29, 30, 31, 32, 33]. Actually, they introduced a global source combined with the jet-drive model valid for thin jets and with the discrete-vortex model valid for tick jets. With an appropriate choice of some fitting parameters, its predictions are in good agreement with experimental results. By balancing the acoustical energy losses due to vortex-shedding at the labium obtained by a semi-empirical method to the acoustic energy produced by the global source, they obtained the relation of $\bar{v}_y/V$ with d/l, where d denotes the high of the flue channel. For example, they found the relation in the jet-driving regime,

$$(\bar{v}_y/V)^2_{max} \approx S_r(d/l)^{3/2} \tag{20}$$

where S_r is the Strouhal number: $S_r = fl/V$. This theory also allows us to reproduce the relation between the jet velocity and the acoustic frequency, like that in Fig.4, though details in calculation were not given in ref. [29].

3 Models and numerical scheme

3.1 Numerical models

In the numerical analysis of flue instruments, we need to simultaneously calculate the dynamics of the jet flow and the acoustic field excited in the resonator. The sound speed c_0 of about 340m/s is much higher than the jet velocity V, which is at most several tens m/s. To reproduce a sound, a much smaller time step is required compared with ordinary numerical calculations of fluid dynamics. On the other hand, the spatial scales required for calculations of fluid dynamics with the eddies, some of which are smaller than 1mm, are much smaller than the wavelength of sound in the physically relevant range –for example, the acoustic wavelength 34mm at frequency 10kHz. Therefore, in the numerical calculation of flue instruments, both requirements, a sufficiently small time step to describe sound propagation and a spatial mesh fine enough to reproduce vortices in fluid, should be satisfied. Further, particle velocities of sound (or energies of sound) are usually much less than those of the flow. Indeed, sound energies are 10^{-4} times smaller than those of fluid in the atmosphere. Thus it is not easy to numerically calculate sound propagation over a long distance with a high degree of accuracy.

To realize the calculation for 2D and 3D model instruments, we concentrate our attention on dynamics in the acoustic near field. Fig.5(a) shows the geometry of the 2D model, which is a small flue organ pipe-like instrument with an end-stop and without a foot ahead of a flue channel, where e and d denote the length and height of the flue channel, respectively, l width of mouth aperture, L pipe length, h pipe height, and their values are taken as indicated in the figure caption. The edge(labium) angle is fixed at 25°, the value at which we got the most stable oscillation in preliminary calculations. This angle value is in a range suitable for real instruments. The model instrument is 90mm in length, and thereby the first acoustic pipe mode frequency is estimated as $f_0 \approx 900$Hz taking into account the open end correction of the 2D open mouth (see Appendix).

The 3D model is formed by adding a uniform width of 10mm perpendicular to the 2D model geometry and holding it between two parallel non-slip solid walls. The 3D model is therefore a quasi-two-dimensional model and the geometry around the mouth-opening is very similar to the instrument used in the experiment by Coltman[13], though it is open at the remote end toward the 3D open space. Since Coltman observed essentially the same relation between the jet velocity and acoustic frequency as that of Fig.4, it is expected that the relation in Fig.4 is observed for the 2D and 3D models.

3.2 Numerical method

The numerical scheme which we use in this work is the compressible LES (Large Eddy Simulation), which is very popular in numerical simulations of aero-acoustics. Specifically, we use a compressible LES solver in the open source software OpenFOAM [59]. In LES the effects of eddies smaller than the grid size are estimated with a statistical model, the so called SGS (sub-grid-scale) model, and are included into the larger scale dynamics of the fluid, thereby making LES very stable for a long

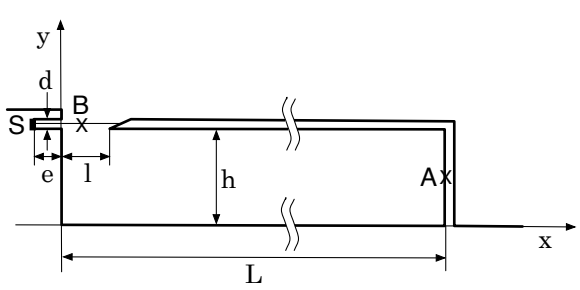

(a) Dimensions of 2D model:$e = 3$mm, $d = 1$mm, $l = 5$mm, $h = 10$mm and $L = 90$mm.

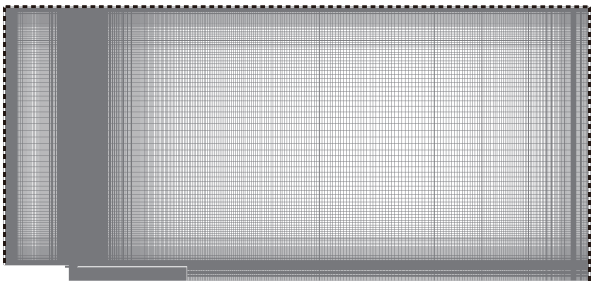

(b) Numerical mesh. Dotted lines denote transparent walls.

Figure 5: (color online) 2D model and mesh.

time simulation. Several SGS models are implemented in OpenFOAM and we use the one equation eddy model [60, 61, 62]. Since the equations for the 2D fluid are derived from the 3D equations by assuming uniformity in the third direction, then the 2D LES scheme used for the calculation of the 2D instrument is obtained in the same way by imposing uniformity of the third direction on the 3D LES scheme. In this way, 2D and 3D LES use the same scheme in OpenFOAM. It has also been reported that the 2D LES scheme can well approximate the dynamics of 2D fluid as well as that of quasi 2D fluid [63].

Note that 2D fluid has particular characteristics that are essentially different from 3D fluid[64, 65, 66]. Namely it has the double cascades in the inertial range: the inverse energy cascade is observed for an upper range above the energy injection scale l_0, while the direct enstrophy cascade exists for a lower range below l_0. The inverse energy cascade generates larger-scale eddies which are considerably robust in time evolution. Then one should take special care in implementing 2D LES. That is, the grid sizes must be taken in the enstrophy cascade range sufficiently smaller than the energy injection scale, otherwise it cannot reproduce large-scale eddies generated by the inverse energy cascade. In our calculation, the energy injection scale is in the order of $10^{-2} \sim 10^{-3}$m, while the grid sizes near the mouth opening are taken small enough in the order of 10^{-4}m. As a result, larger scale eddies are generated for 2D simulations as shown latter. For more rigorous calculations, the direct numerical simulation(DNS) is suitable, but it requires a finer mesh, which is equal to or less than the Kolmogorov length scale estimated as $l_k = l_0 Re_t^{-3/4} \approx O(10^{-5}) \sim O(10^{-6})$m, where Re_t denotes the turbulence Reynolds number, and the calculation time becomes $10^2 \sim 10^4$ times longer than the LES scheme. Then DNS requires large computing resources and is unrealistic for our computational resources, as discussed below. This is one of the reasons why we choose LES rather than DNS in this paper, although LES has less reproducibility. Another reason for use of LES is the good reproducibility of acoustic fields including open end reflections[40, 42].

Fig.5(b) shows the numerical mesh of the 2D model, which has an area of 450×200mm^2 – large enough to include the acoustic field outside the instrument and for vortices to substantially decay before reaching boundaries. The upper, right and left sides of the mesh are transparent walls, while the other boundaries are non-slip solid walls. The Poinsot-Lele method is used to achieve the transparent boundary condition [67]. To make the Poinsot-Lele method work well, we take a finer mesh with an interval less than 1mm near the transparent walls. Parameters of the 2D and 3D meshes are taken as shown in Table 1. For the 3D model, 50 grid points are taken between the two solid walls between which the instrument is held. It may be necessary to take a finer mesh for more accurate calculations, but this is almost the limit of our computational ability at present.

The pressure and temperature at rest are taken as $p_0 = 100$kPa and $T_0 = 300$K, respectively. The time step of the numerical integration is $\Delta t =$

Table 1: Parameters of 2D and 3D meshes

Model	Points	Cells	Faces
2D	158,762	78,492	314,856
3D	4,048,431	3,924,600	11,896,692

10^{-7}sec. For the 2D model, time evolution up to 0.1sec is calculated. The velocity of the jet emanating from the flue V in the range $(2 \leq V \leq 40\mathrm{m/s})$ is taken as a control parameter. On the other hand, the time evolution of the 3D model is calculated up to 0.03sec at $V = 12\mathrm{m/s}$ and $V = 36\mathrm{m/s}$. The reason why the 3D calculation is done for a shorter time than the 2D calculation is that the 3D calculation requires a much longer computation time even with parallel processing. Indeed, the 3D calculation of 0.03sec using 10 parallel threads in an Apple MacPro (2.93GHz, 6 Core Intel Xeon"Westmere"$\times$2) takes about 30 days and the resultant data exhausts a disk volume of more than 1TB even after compression.

The input flow with a uniform velocity V is injected from the surface S at the left end of the flue in Fig.5(a). It is started impulsively at $t = 0$s, then shock waves are generated with very high frequencies associated with the flue channel pipe resonance. But they reduce in a very short time mostly within 5×10^{-3}sec. Since the flue is short in length, 3mm, then a jet of a top hat profile is expected in a stationary regime[47, 68], but the jet profile obtained numerically at the flue exit is an intermediate one between top hat and Poiseuille velocity profiles independent of grid choice. This is perhaps due to lack of a foot(small chamber) supplying the air to the flue channel. Since the behavior of the jet with a bell shaped profile is more stable with change of V and with acoustic field disturbance than the jet with a top hat profile[47, 68], then the jet of our models is expected to be fairly stable.

Observations of pressure fluctuation$(= p - p_0)$ and vorticity are made at the following points. The pressure fluctuation is observed at the point A in Fig.5(a), the center of the right end of the pipe. The vorticity in the jet flow is calculated at point B at a distance of 2.0mm right from the exit of the flue and on the extension of the center line of the flue.

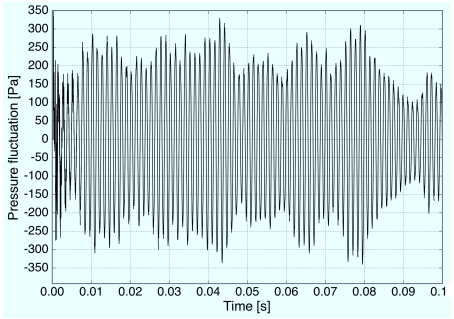

(a) Pressure fluctuation at point A in Fig.5(a).

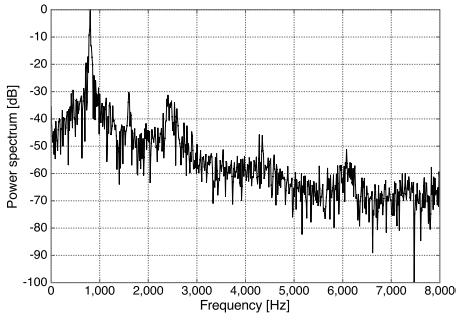

(b) Power spectrum.

Figure 6: Pressure fluctuation at V=12m/s in the 2D model.

4 Numerical results

4.1 Stable oscillation at $V = 12$m/s

4.1.1 Pressure fluctuation at the closed end

In this subsection, we compare numerical results for the 2D and 3D models at $V = 12\mathrm{m/s}$, the value in the whole range of V at which the most stable oscillation is observed for the 2D model. Fig.6 shows the pressure fluctuation observed at the point A for the 2D model and its power spectrum, respectively. For the calculation of the spectrum, initial transient oscillation $(0 \leq t < 0.01\mathrm{s})$ is omitted. In Fig.7, the change of the pressure fluctuation at the point A for the 3D model and its power spectrum are plotted, respectively. The spectrum is calculated from the data in the range $(0.005 \leq t \leq 0.03\mathrm{s})$. For the sake of comparison, the result of the 2D model (dotted line) is superposed in Fig.7(a).

The pressure fluctuation of the 2D model in Fig.6(a) is stable with an almost constant pitch throughout the whole range of time $(0 \leq t \leq 0.1\mathrm{s})$, except for a short initial transient. As shown in

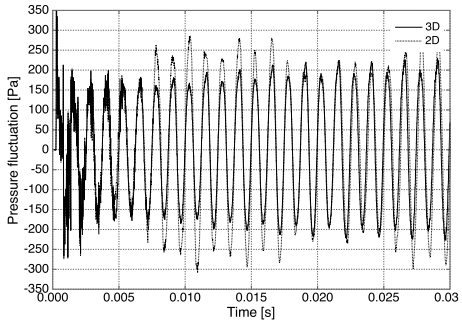

(a) Pressure fluctuations of the 3D model(solid line) and the 2D model(dotted line) at point A in Fig.5(a).

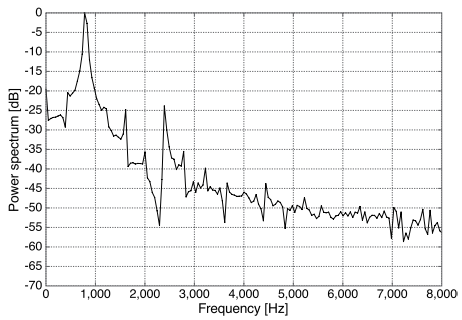

(b) Power spectrum of pressure fluctuation in the 3D model

Figure 7: Comparison of pressure fluctuation at V=12m/s in the 3D model with that in the 2D model.

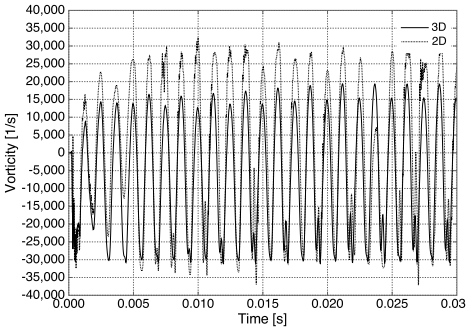

(a) Vorticity of the 3D model(solid line) and the 2D model(dotted line) at point B in Fig.5(a).

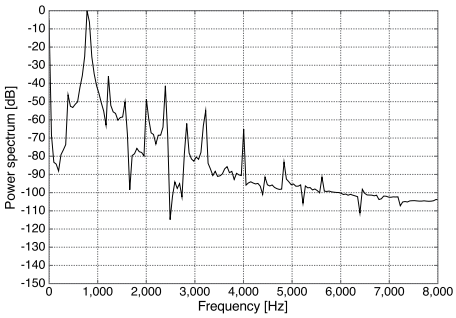

(b) Power spectrum of vorticity in the 3D model.

Figure 8: Comparison of the jet vorticity at V=12m/s in the 3D model with that in the 2D model.

Fig.7(a), the pressure oscillation of the 3D model almost coincides with that of the 2D model up to 0.007s, but after that it is more stable than the 2D result. The oscillation amplitude of the 3D model is about 200kPa and very stable, while the amplitude of the 2D oscillation is gently undulating.

The oscillation amplitudes in the resonator produced numerically are much larger than normal acoustic pressures in the open air field and they have clear pitches near the fundamental frequency of the resonator. Then it is considered that the acoustic oscillations in resonance are observed for both 2D and 3D models.

As shown in Fig.6(b) and Fig.7(b), the main peaks of the spectra of the 2D and 3D oscillations are very sharp and respectively appear at $f =$ 806Hz and $f = 795$Hz, which are close to each other. We can understand the reason why the frequencies of the excited waves for the 2D and 3D models take almost the same values. Since the distance between the two boundary walls of the 3D model is only 10mm, then the acoustic wave of a frequency less than 17000Hz behaves like a 2D wave and the end correction for the 3D wave is well estimated by the 2D end correction in the physically relevant frequency range (even though the flow dynamics are quite different between the 2D and 3D models, as will be shown later).

For the reason given above, we are able to use the 2D model at least to evaluate the frequency of an excited wave in the 3D resonator at a given jet velocity, ignoring details of the wave form. The frequency of the wave at $V = 12\mathrm{m/s}$ is less than the theoretical estimation of the first acoustic pipe mode frequency of the 2D model, 900Hz (see Appendix A), by about 100Hz. However, the frequency of the 2D model (probably as well as that of the 3D model) rapidly approaches the resonance frequency with increase of V, as shown later (see Fig.12). Thus it is considered that the oscillations

at $V = 12\mathrm{m/s}$ for both 2D and 3D models are almost locked on the fundamental resonance.

4.1.2 Synchronization of the jet flow with the acoustic oscillation

Figs.8 (a) and (b) show the change of z-component of the vorticity observed at the point B in the jet for the 3D model and its power spectrum, respectively. For the sake of comparison the vorticity of the 2D jet is also shown by a dotted line in Fig.8(a). At the point B on the extension of the center line of the flue, the vorticity takes rather small values (see Figs.9(f) and 10(b)), but it switches between positive values and negative values with the jet oscillation. So it shows the jet oscillation more clearly than the direct measurement of the jet velocity. The vorticity regularly oscillates like the acoustic pressure at the point A with the same fundamental frequency, as seen in the power spectrum (see Fig.8(b)). Therefore, the jet oscillation is well synchronized to the resonance oscillation of the acoustic pressure in the pipe, though like the pressure oscillations, the vorticity in the 2D model is rather more unstable than that in the 3D model.

4.1.3 Spatial distributions of characteristic dynamical variables

Let us see the spatial distributions of dynamical variables which characterize the flow dynamics and acoustic oscillation. The left column of Fig.9 shows spatial distributions of acoustic pressure, absolute value of flow velocity, vorticity and Lighthill's source at a certain time for the 2D model. The right column of Fig.9 shows spatial distributions of the same dynamical variables for the 3D model, except for the vorticity which is replaced by the z-component of the 3D vorticity vector. We used eqs.(3) and (6) for the calculations of Lighthill's sources for the 3D and 2D models, respectively.

In the stationary oscillation regime, the fluctuations of pressure become much larger in amplitude inside the pipes than outside, and oscillate periodically for both 2D and 3D models (see Figs.9(a), 9(b)). So, it is confirmed that they are in resonance and make a strong acoustic field in the pipe. There are rather complicated distributions near the mouth opening for both models, which are a superposition of the acoustic pressure and local pseudo sound pressure (or hydrodynamic pressure)[24].

In the velocity distributions in Figs.9(c) and 9(d), the jets oscillate periodically with the same pitches as the acoustic pressure for both 2D and 3D models. The velocity distribution on the cross section of the pipe through the top of the edge together with the magnified picture near the open mouth is shown in Fig.10. The jet colliding with the edge creates eddies going alternately to the upper and lower sides of it. However, the eddies behave in different ways for the 2D and 3D models.

For the 2D model, after the eddies are created by the collision of the jet with the edge, they soon roll up and form clear vortex tubes and persist for considerably long times. Eddies outside the instrument gradually separate from the wall of the pipe and stagnate on an upper side. On the other hand, those inside the instrument are reduced to a large rotor or a few rotors near the open mouth, which never spread further into the right hand side. Actually no eddies apparently appear in the right 2/3 part of the pipe, in which absolute values of the velocity $|\boldsymbol{v}|$ in the stable oscillation are less than p_{max}/c_0, where p_{max} is the maximum pressure observed at the point A, so that the strong acoustic field dominates the flow in this region. The existence of the long-life eddies and large rotors is considered to be a result of the characteristic of 2D flow, i.e., the inverse energy cascade[64, 65, 66]. The eddies and rotors considerably affect and disturb the dynamics of the jet as well as the acoustic field in the pipe so that they often become unstable undulating amplitudes.

For the 3D model, the eddies created near the edge break up into lumps of turbulence, i.e., smaller scale eddies, in a short time (see Fig.10). The lump outside the instrument moves along the upper wall. The lump inside is stagnant and localized in the area near the open mouth and never forms a large rotor (or rotors). Like the 2D model, no eddies and no local turbulence apparently appear in the right 2/3 part of the pipe, where the relation $|\boldsymbol{v}| < p_{max}/c_0$ is satisfied in the stable oscillation, so that the strong acoustic field dominates the flow in this region.

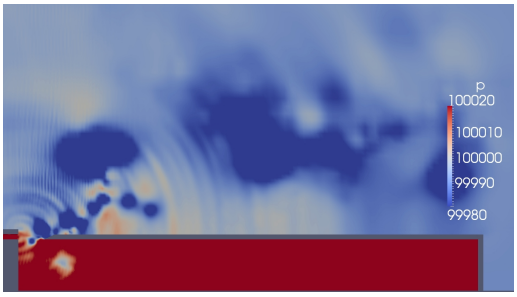

(a) Pressure. 2D

(b) Pressure. 3D

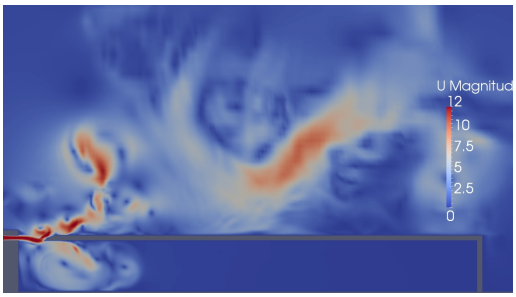

(c) Magnitude of flow velocity. 2D

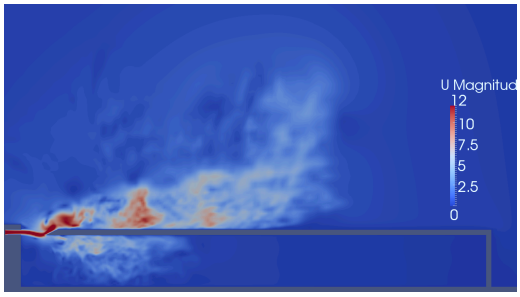

(d) Magnitude of flow velocity. 3D

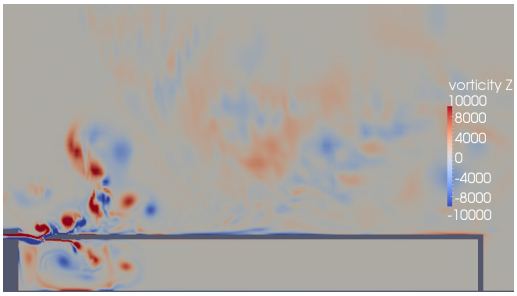

(e) Vorticity. 2D

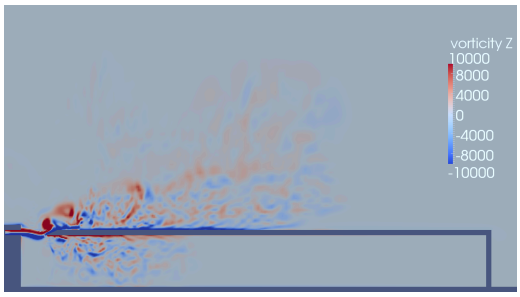

(f) Z-component of vorticity. 3D

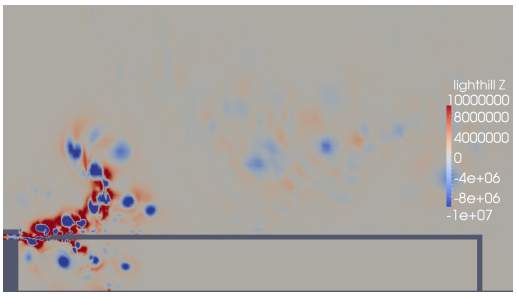

(g) Lighthill's source. 2D

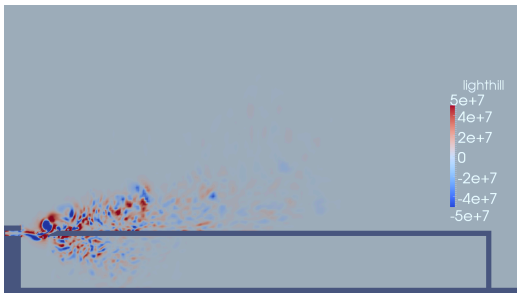

(h) Lighthill's source. 3D

Figure 9: (color online) Spatial distributions of representative dynamical variables at $V = 12\mathrm{m}/\mathrm{s}$ for the 2D and 3D model. In the case of 3D, they are the vertical cross section along the center line of the 3D instrument and parallel to the $x-y$ plane.

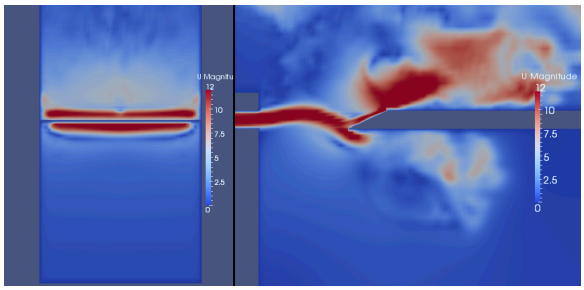

(a) Magnitude of flow velocity

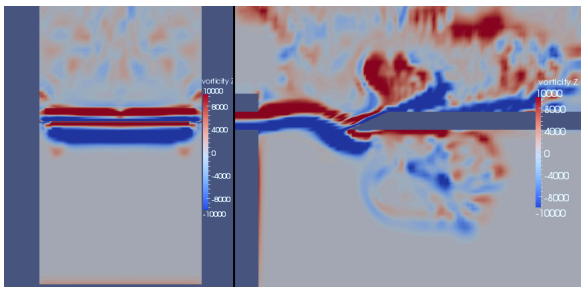

(b) Z-component of vorticity

Figure 10: (color online) Velocity and vorticity distributions: the left pictures are those on the cross section through the top of the edge and perpendicular to the $x-y$ plane, and the right pictures are the magnified pictures near the open mouth on the same cross section as that of the 3D pictures in Fig.9.

In general, because of the characteristic of 2D fluid, i.e., the inverse energy cascade, a vortex tube in 2D fluid is more robust than that in 3D fluid and a rolled up eddy survives for a longer time in the 2D simulation than the 3D simulation. In the 2D model, the well rolled up eddies often disturb the jet motion and acoustic field due to their irregular behavior. In other words, the absence of strongly rolled up eddies means that the oscillations are more stable in the 3D model.

Another 3D effect on the jet is also observed in the cross-section of the pipe through the top of the edge in Fig.10(a). Namely, even when the major part of the jet flows into the cavity under the edge, fluid particles in the thin layers close to both boundary walls are almost at rest and remain near the upper side of the edge. A similar 3D effect was also reported in Ref.[37].

Figs.9(e) and 9(f) show the vorticity distributions for the 2D and 3D models, respectively. As clearly seen in Fig.9(e), the vorticity takes a positive or negative value at the center of an eddy depending on its rotational direction, though the pressure displacement($= p - p_0$) always takes a negative value at the center of an eddy (see Fig.9(a)). For the 3D model in Fig.9(f), the same tendency is observed, but there is a rather irregular distribution in the lumps of turbulence. On the other hand, the vorticity along the jet takes positive and negative values along its upper and lower parts, respectively, for both 2D and 3D models. Fig.10(b) shows the close-up view near the mouth opening and the cross section of the pipe through the top of the edge. The distribution of the vorticity clearly changes at the top of the edge. In the upper stream, it forms double layers of positive and negative values, but when it passes across the top of the edge, it bifurcates and separates, due to unsteady force of the top of the edge to the jet flow, into a pair of double layers on upper and lower sides of the edge. The bifurcation induces successive vortex shedding and probably contributes to the generation of acoustic pressure.

As seen in Figs.9(g) and 9(h), the distributions of Lighthill's sources appear to approximately overlap with the vorticity distributions for both 2D and 3D models. In the 2D distribution, a rolled up eddy always takes a negative value at its center and takes positive values along its circumference. However, in the lump of turbulence observed in the 3D distribution, it is distributed in a complicated way.

Lighthill's source along the jet makes a different pattern from that of vorticity, reflecting the difference of geometry between the fluid flow structures, and seems to be more complicated for both 2D and 3D models. As shown by the magnified picture near the open mouth of 3D model as well as the schematic picture in Fig.11, for a part of the jet wave with a positive slope, it seems to take negative and positive values along the upper and lower parts, respectively. But, for anther part with a negative slope, it takes the opposite pattern: positive along the upper part and negative along the lower. The same characteristic pattern along a jet is also observed for a purely edge tone model without a cavity [40, 42]. Further, there is a characteristic dis-

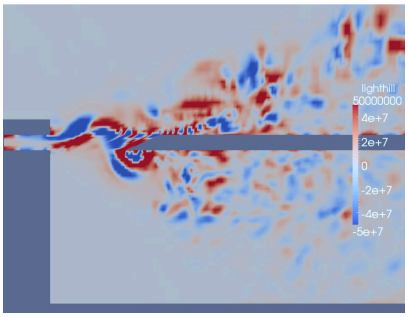

(a) Magnified picture near the open mouth for the 3D model.

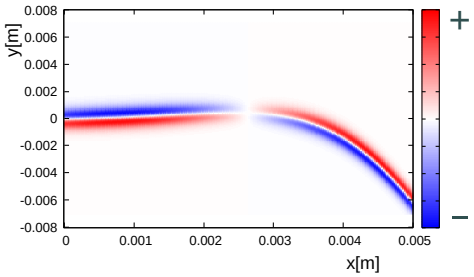

(b) Schematic picture of the distribution along a jet.

Figure 11: (color online) Lighthill's source distribution along the jet. The picture in (a) is a snap shot at a different time from that in Fig.10. The origin of the coordinate in (b) is taken at the middle of flue exit.

tribution just below the top of the edge due to the collision of the jet with it, which might be related with the jet-drive model and/or the discrete-vortex model in refs.[5, 13, 28, 29, 30, 31, 32, 33].

The major pressure sources are located in the areas of strong vorticity, namely along the jet, in the eddies and in the lump of turbulence. This result qualitatively agrees with the Powell-Howe vortex sound theory [6, 25, 26]. Therefore, the sound production is associated with those vortex-shedding and moving vortices, but it should be considered that the sound is generated by the entire flow, because the Lighthill source is related in a complicated way with not only the acoustic pressure but also the local pseudo sound pressure (or hydrodynamic pressure)[24].

Note that Fig.11(b) only shows a schematic picture of Lighthill's source along the jet, but its central line is obtained with eq.(9) at $f = 795$Hz, $\omega = 2\pi f$, $V = 12$m/s, $u = V/2$, $\mu = k = \omega/u$ and $\bar{v}_y/V = 0.08$. For the estimation of $\bar{v}_y$ the approximation $\bar{v}_y \approx p_{max}h/\rho_0 C_0 V l$ given in ref.[31] is used, where p_{max} indicates the amplitude of the pressure fluctuation at the point A and is taken as $p_{max} \approx 200$Pa, and $h = 10^{-2}$m, $\rho = 1.23$kg/m^3, $c_0 = 348$m/s and $l = 5\times 10^{-3}$m. The jet profiles obtained numerically and theoretically are quite different to each other. The jet of the numerical calculation has an arc-shaped profile, while that obtained theoretically goes upward slightly in the left half and goes down exponentially in the right half. The jet profile obtained numerically is very similar to that observed experimentally in a low jet velocity range[30]. Therefore, this discrepancy indicates the incompleteness of the theory, which is mainly due to the fact that the existence of the edge is ignored in framing the jet model. It is also assumed in the jet model that a uniform acoustic flow goes through the mouth, but it is actually non-uniform and probably takes the maximum value near the flue exit, which bends the jet just after leaving the flue exit [29]. Thus the unphysical jet model may induce some inaccuracy in prediction of the frequency of an acoustic oscillation for a given jet velocity, as discussed later.

4.2 Frequency change with jet velocity

4.2.1 Numerical results: switching between synchronization and desynchronization to the acoustic pipe modes

In this subsection, mainly using the 2D model, we discuss changes of characteristic frequencies of acoustic waves excited in the pipe, namely, the fundamental and first overtone peaks of the spectrum of the pressure fluctuation at the point A, with increase of the jet velocity V. In Fig.12, we show the characteristic frequencies of the pressure fluctuation at the point A as a function of V in the range ($2 \le V \le 40$m/s) for the 2D model. In Fig.12, we also show the results for the 3D model marked by an X at $V = 12$ and 36. For the sake of comparison, the resonance frequencies of the pipe estimated theoretically(Appendix) and the edge tone frequency given by eq.(8) with $j = 1$ are also depicted in Fig.12. The fundamental frequency is observed in the whole range of V, but the first overtone appears only at high velocities, $V \ge 18$m/s.

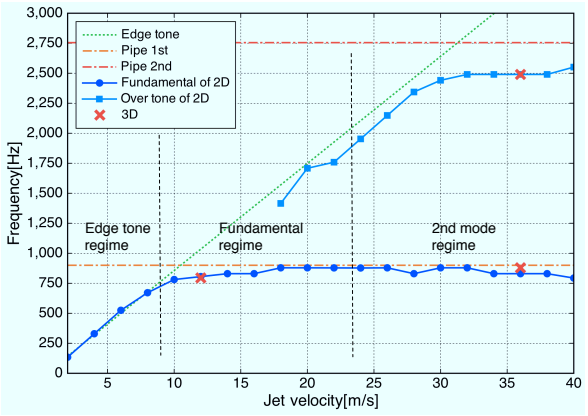

Figure 12: (color online) Changes of oscillation frequencies with jet velocity. The lines labeled 'Pipe 1st' and 'Pipe 2nd' indicate the theoretical estimates of the frequencies of the first and second acoustic pipe modes, respectively.

In the low velocity regime ($V \leq 8\mathrm{m/s}$), the pressure fluctuation is small, not exceeding several tens Pa, and the increase of its fundamental frequency is similar to that of the edge tone(the first hydrodynamic mode), namely it is proportional to V. Because the jet motion is little affected by the acoustic pipe mode, it almost keeps the natural oscillation of the edge tone.

In the middle range ($10 \leq V \leq 22\mathrm{m/s}$), pressure oscillations locking on the first acoustic pipe mode(the fundamental resonance) are observed for the 2D model. Like the case of $V = 12\mathrm{m/s}$ in the previous subsection, it is well expected that similar resonance oscillations are observed for the 3D model in this range. The oscillation frequency at $V = 10\mathrm{m/s}$ is fairly low compared to that of the first acoustic pipe mode(theoretical prediction), but it quickly approaches the first acoustic pipe mode frequency with increase of V. The oscillations are very stable in the range ($10 \leq V \leq 16\mathrm{m/s}$) and the most stable one is observed at $V = 12\mathrm{m/s}$, as mentioned in the previous subsection. It turns out that the oscillation is most stable just after the jet motion starts synchronizing with the pipe resonance.

However, though we do not show results here, oscillations become slightly unstable in the range ($18 \leq V \leq 22\mathrm{m/s}$), with amplitude modulations sometimes occurring in long term evolutions. In the spectra of these oscillations, there appears a peak corresponding to the edge tone frequency at the given velocity V. Further smaller peaks whose frequencies are nearly equal to the third harmonic of the pipe are often observed. It is considered that competition among the resonances of the pipe and the edge tone, i.e., inherent oscillation of the jet, occurs, but the fundamental still dominates the others, though its oscillation is somewhat disturbed. Since the transition between the first acoustic mode and the second is in general quite unstable in musical instruments, it is considered that the system vacillates between the two solutions in this range, i.e., so called "warble" occurs[50].

The frequency of the first overtone peak increases mostly in proportion to the jet velocity, like the edge tone(hydrodynamic mode), in the range $18 \leq V \leq 28\mathrm{m/s}$ but it converges to almost a constant value in the range $V \geq 32\mathrm{m/s}$, e.g., $f_1 = 2490\mathrm{Hz}$ at $V = 36\mathrm{m/s}$, although it is considerably lower than the theoretical estimation of the second acoustic pipe mode frequency(the third harmonic), 2755Hz. Unfortunately, we do not know the reason for the discrepancy between the theoretical prediction and the observed values, but it might be explained by the effect of the weakness of the second acoustic resonance mode due to the small reflectance of the 2D acoustics(see Appendix). In the high velocity range ($V \geq 24\mathrm{m/s}$), first overtone peaks likely to be the second acoustic mode are clearly observed in the spectra of pressure fluctuation. Indeed, the peak height of the first overtone is increasing with V and becomes larger than that of the fundamental for $V \geq 24\mathrm{m/s}$. Further the wave form of pressure fluctuation changes to that of the second acoustic mode for $V \geq 24\mathrm{m/s}$. Then the oscillation starts to be synchronized with the second acoustic pipe mode around $V = 24\mathrm{m/s}$. Fig.13(a) shows the change of pressure fluctuation at the point A for the 3D model at $V = 36.0\mathrm{m/s}$ compared with that for the 2D model. The pressure fluctuation of the 3D model oscillates almost periodically with a very large amplitude around 1kPa, while that of the 2D model is slightly unstable. As shown in Fig.13(b), the spectrum peak corresponding to the second acoustic mode is apparently larger than the fundamental peak. Thus the oscillation is of the second acoustic mode.

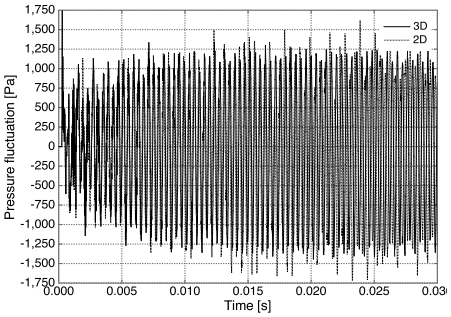

(a) Pressure fluctuations of the 3D model(solid line) and the 2D model(dotted line) at point A in Fig.5(a)

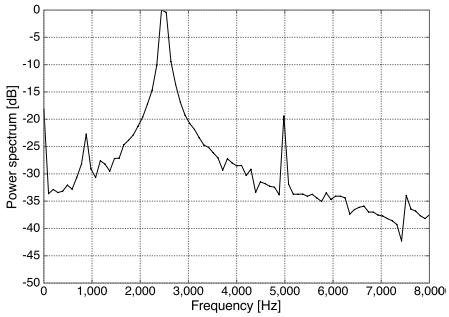

(b) Power spectrum of pressure fluctuation in the 3D model.

Figure 13: Comparison of pressure fluctuation at at $V = 36\mathrm{m/s}$ in the 3D model with that in the 2D model.

In conclusion, the characteristic frequencies of the 2D model almost coincide with those of the 3D model at the two representative values of the jet velocity, $V = 12,\ 36\mathrm{m/s}$. Therefore, it is reasonable to consider that the characteristic frequencies of the oscillations excited in the 3D resonator are well estimated by using the 2D model in the physically relevant range of the jet velocity. However, the details of the wave forms are quite different between the 2D and 3D models and the oscillation of the 3D model is more stable than that of the 2D model.

4.2.2 Comparison with the semi-empirical theory

Let us compare our numerical result with the theoretical prediction introduced in section 2.3. Fig.14 shows the velocity-frequency curves (red broken lines) given by eq.(19), for which parameters are adjusted to match our numerical calculation: $l =$

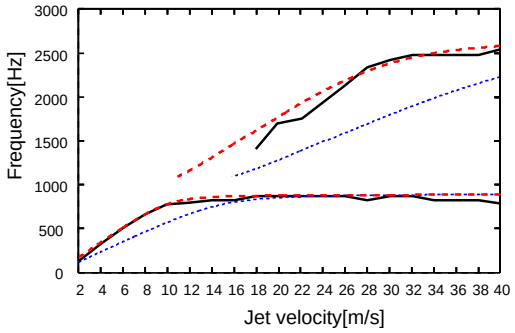

Figure 14: (color online) Comparison of the numerical result with the theoretical prediction for change of frequencies with the jet velocity.

5mm, $\Delta L_m = 13\mathrm{mm}(\approx 2\Delta L_{2D}$ at 1000Hz), $h = W = 10\mathrm{mm}$, $S_p = hW$, $S_m/S_p = 0.95$, $L = 90\mathrm{mm}$, $c_0 = 348\mathrm{m/s}$, $\bar{k} = \omega/u$ and $\mu = \bar{k}$ (see Fig.5(a)). We rescale the argument of the exponential function in eq.(13) as $u = 0.73V$ to adjust it to the edge tone equation (8) and also to our numerical result, while it is usually taken as $u \leq 0.5V$. For comparison, the velocity-frequency curves obtained numerically in Fig.12 are shown again by solid lines.

Our numerical result shows good agreement with the theoretical prediction in three characteristic ranges: the edge-tone-like oscillations in the low velocity range, the oscillations locking to the fundamental acoustic resonance in the middle range, and the transition to the second acoustic mode in the high range.

Finally, we explain the reason why the parameter u is taken as $u = 0.73V$ instead of $u = 0.5V$ in order to calculate the velocity-frequency curves. According to experiments and the semi-empirical theory, the phase velocity u of the jet wave should take a value in the range $u \leq 0.5V$[1]. However, we have to remind the fact that the existence of the edge is ignored in framing the jet model in the theory (see Section 2.3) and it significantly affects the jet motion. Actually, as shown in Fig.11 and as discussed in subsection 4.1.3, the theoretical prediction is quite different in jet profile from the numerical results as well as experimental results[30]. Further, it is reported that at the low velocities at which the edge-tone dominates, the model of eq.(9) fails, because the jet rolls up into discrete vortices

before reaching the edge of the mouth[33]. Therefore it is probably necessary to modify the parameter to some extent. Indeed, the velocity-frequency curves given at $u = 0.5V$ by eq.(19)(see blue dotted line in Fig.14) tend to the right more and apparently deviate from our numerical results as well as Brown's edge tone equation. Namely, the curves are markedly shifted from the edge tone line in a low velocity range and the onset point of locking to the fundamental is estimated as $V \approx 16\mathrm{m/s}$. Then, the choice of the parameter value $u = 0.73V$ is necessary to get quantitative agreement with the full numerical calculations.

4.3 Acoustic flow through the mouth opening vs. jet velocity

In this subsection, we discuss the rate of acoustic particle velocity through the mouth to the jet velocity, which allows us to estimate the energy transfer rate from hydrodynamic energy to acoustic energy[3, 29, 30, 31, 32, 33]. The acoustic particle velocity is simply evaluated as[31]

$$\bar{v}_y \approx p_{max} h / \rho c_0 l. \tag{21}$$

The amplitude of the pressure fluctuation at the closed end p_{max} is taken as $p_{max} \approx 200\mathrm{Pa}$ at $V = 12\mathrm{m/s}$ and $p_{max} \approx 1\mathrm{kPa}$ at $V = 36\mathrm{m/s}$, then the dimensionless amplitude $\bar{v}_y/V$ is estimated as $\bar{v}_y/V \approx 0.08$ and $\bar{v}_y/V \approx 0.14$, respectively. On the other hand, it was reported in ref. [3] that $(\bar{v}_y/V)_{max} \approx 0.3$ at $l/d = 5$ for recorder type instruments. In the experiments[30, 31, 32, 33], it is in the range $0.25 \leq (\bar{v}_y/V)_{max} \leq 0.3$ at $l/d = 4$ for organ pipes and whistle(or ocarina)-type instruments. Comparing with the values obtained experimentally for the real instruments, those obtained by the numerical calculations for 2D and 3D models are considerably small.

We consider the following two reasons to explain this discrepancy. First, we do not evaluate the maximum value of $\bar{v}_y/V$, though the maximum value $(\bar{v}_y/V)_{max}$ is used in refs.[30, 31, 32, 33]. Indeed, we calculated only two cases: the first acoustic mode at $V = 12\mathrm{m/s}$ and the second acoustic mode at $V = 36\mathrm{m/s}$ for the 3D model. For the 2D model, we observed a pressure beyond 1kPa at $V = 22\mathrm{m/s}$, though it is a little unstable, so that $\bar{v}_y/V \approx 0.21$, but it is still smaller than those obtained experimentally for the real instruments. It may be attributed to the difference of geometry between the real instruments and the numerical model. Namely $(\bar{v}_y/V)_{max}$ seems to depend on the geometry of the mouth piece. For example, flute type instruments take a larger value, $(\bar{v}_y/V)_{max} \approx 0.35$ at $l/d = 5$ compared with the recorder type instruments[3]. The 3D model in this paper has a mouth piece of quasi-2D geometry for acoustic waves, which is similar to that of the instrument studied experimentally by Coltman[13]. The reflectance at the mouth for the 2D and quasi-2D instruments is quite smaller than that of real 3D instruments and the smaller reflectance reduces the value of $(\bar{v}_y/V)_{max}$. Further, the difference of the fluid structure near the mouth piece due to the difference of geometry may induce an additional energy loss of acoustic energy. However, the detailed study of this issue is postponed to a future work.

5 Summary and discussion

In this paper, we have reported on the numerical analyses of 2D and 3D flue organ pipe like instruments with the compressible LES. The 3D model is a quasi-2D model consisting of a volume between two parallel non-slip walls, whose geometry near the mouth opening is similar to that studied experimentally by Coltman[13]. Therefore, the 3D model has two dimensional character in acoustics but has three dimensional character in fluid dynamics.

Results show that the oscillation of the instruments are well reproduced by using the compressible LES. Even for the 2D model, the characteristic feature of flue instruments reported in refs.[1, 13, 14, 19, 20, 30] is well reproduced, namely the acoustic oscillation changes with increase of the jet velocity as follows: the edge-tone-like oscillations in the low jet velocity range, the oscillations locking to the fundamental acoustic mode in the middle range, and the transition to the second acoustic mode in the high range.

Comparing the 2D and 3D models, the 2D model is more unstable due to the characteristic of 2D fluid. Namely, for the 2D model there exist long-life vortex tubes, whose irregular behavior

near the mouth opening often disturbs the jet motion as well as the acoustic field passing through it. Therefore, a 3D simulation is hydrodynamically important because it avoids spurious jet instabilities.

Concerning the amplitude of acoustic waves excited in the resonator, the quasi-2D model (and 2D model) tends to take smaller values compared with those observed for the real 3D instruments. This is because of the 2D acoustic nature of the quasi-2D model in the physically important frequency range, namely a weak reflectance reduces the resonance amplitude. Therefore, simulation of a model of the complete 3D acoustic nature is important in order to reproduce typical oscillation amplitudes and associated non-linearity found in flue instruments, though it requires an extremely huge computation cost necessitating the use of a high performance super-parallel computer.

In order to pursuit the acoustic mechanism of flue instruments in terms of aerodynamic sound together with to reproduce the far-field acoustics, handling Curle's integral formula based on Lighthill's analogy is very important. As discussed in subsection 2.1, there are some difficulties in applying Curle's formula to the case of flue instruments due to the existence of the strong acoustic field in the resonator. So we did not discuss the Curle's formula in this paper. Instead of using the Green function, a hybrid method of fluid solver and acoustic solver may be practically useful to reproduce the far field acoustics[55].

An alternative way to estimate the energy transfer between the acoustic field and the hydrodynamic field was proposed by Howe[27]. To apply Howe's formula, it is necessary to separate the acoustic field from the hydrodynamic field with sufficient accuracy. However, there is no established method to do it in a direct way. On the other hand, there are some experimental strategies (or hybrid methods combining measurement with numerical calculation) to estimate the acoustic field by using an external driving source, e.g., loud speaker in non-hydrodynamic field[48, 49, 56, 57]. It is perhaps possible to implement a similar approach in numerical calculations by introducing a virtual external driving source, which would allow us to apply Howe's formula.

Acknowledgments

The authors thank Prof. Yasuhide Fukumoto for discussions on LES and the characteristics of 2D fluid. This work is supported by Grant-in-Aid for Exploratory Research No.20654035 and Scientific Research (C) No.23540455 from Japan Society for the Promotion of Science (JSPA) and is also supported by JHPCN and STPF.

A Reflections from 2D and 3D flanged pipes

In this appendix, we theoretically calculate the radiation impedance of a 2D flanged pipe in the same way as for a 3D flanged pipe[41, 42, 58] and compare some characteristic properties of the 2D open end reflection with those of the 3D reflection.

A spherical wave caused by a 2D point source with a strength Q is given by

$$p(r) = \rho_0 c \frac{Qk}{2} H_0^{(2)}(kr) \mathrm{e}^{i\omega t}, \tag{22}$$

where $H_0^{(2)}$ is the 0-th order Hankel function of the second kind. Superposing 2D spherical waves emanating from sources distributed over the cross section of the open end according to the Huygens-Fresnel principle, we obtain the radiation impedance of the 2D flanged pipe with a height $h = 2a$,

$$\begin{aligned} Z_R^{2D}(\omega) &= Z_0^{2D} \frac{k}{a} \int_0^a dr' \int_0^{2r'} dr H_0^{(2)}(kr) \\ &= Z_0^{2D} \frac{\pi k}{a} \int_0^a dr' r' \\ &\quad \times \Big(\mathbf{H_0}(2kr') H_1^{(2)}(2kr') + \\ &\quad \mathbf{H_{-1}}(2kr') H_0^{(2)}(2kr') \Big), \end{aligned} \tag{23}$$

where $\omega = ck$, the characteristic impedance of the 2D pipe is defined by $Z_0^{2D} = \rho_0 c/2a$ and $\mathbf{H_n}$ denotes the Struve function. In the low and high frequency limits, $Z_R^{2D}(\omega) = R_{2D}(\omega) + iX_{2D}(\omega)$ is respectively

reduced to

$$\lim_{\omega\to 0} Z_R^{2D}(\omega) \approx Z_0^{2D} ka - iZ_0^{2D}\frac{2}{\pi}ka\left(\log(ka)+\gamma-\frac{3}{2}\right) \to 0, \quad (24)$$

$$\lim_{\omega\to\infty} Z_R^{2D}(\omega) \to Z_0^{2D} + O(1/\omega), \quad (25)$$

where γ is the Euler constant. The radiation impedance of an open end pipe without flanges given by ref.[69] is represented in our notation as $Z_R^{2D}(\omega) \approx Z_0^{2D} ka - iZ_0^{2D}\frac{2}{\pi}ka(\log(ka)+\gamma-\log 2\pi-1)$ in the low frequency regime. The difference in the subdominant terms of $O(ka)$ in the imaginary parts comes from the difference of the geometry between flanged and non-flanged pipes.

On the other hand, the real and imaginary parts of the radiation impedance of a 3D flanged pipe $Z_R^{3D}(\omega) = R_{3D}(\omega) + iX_{3D}(\omega)$ is given by[1, 58]

$$Z_R^{3D}(\omega) = Z_0^{3D}(1 - J_1(ka)/ka + i\mathbf{H}_1(2ka)/ka), \quad (26)$$

where J_1 is 1-st order Bessel function and the 3D characteristic impedance is given by $Z_0^{3D} = \rho_0 c/(\pi a^2)$. In the limit of $\omega \to 0$, this is approximated by

$$\lim_{\omega\to 0} Z_R^{3D}(\omega) \approx Z_0^{3D}\left(\frac{(ka)^2}{2} + i\frac{8ka}{3\pi}\right) \to 0, \quad (27)$$

and in the limit of $\omega \to \infty$, Z_R^{3D} converges to Z_0^{3D}.

Fig.15 shows the real and imaginary parts of the 2D and 3D radiation impedance Z_R^{2D} and Z_R^{3D} normalized by the 2D and 3D characteristic impedance Z_0^{2D} and Z_0^{3D} respectively. In the limit of $ka \to 0$, the imaginary part of Z_R^{2D} decays as $\propto ka\log ka$, while the imaginary part of Z_R^{3D} is proportional to ka.

The reflectance is defined by[1]

$$\mathcal{R}(\omega) = \left|\frac{Z_R - Z_0}{Z_R + Z_0}\right|^2, \quad (28)$$

which gives the reflectance of a loss-less pipe, where Z_R indicates the 2D or 3D radiation impedance obtained above. In a low frequency range, $\mathcal{R}$ is approximated as $\mathcal{R} \approx 1 - 4R_{2D,3D}/Z_0^{2D,3D}$: $\mathcal{R} \approx 1 - 4ka + O(k^2a^2)$ for 2D

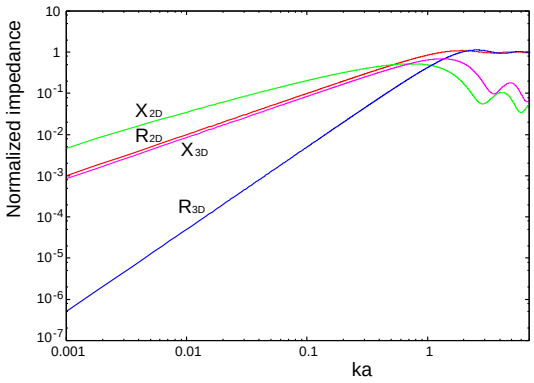

Figure 15: (color online) 2D and 3D radiation impedance normalized by $Z_0^{2D,3D}$. $R_{2D,3D}$ and $X_{2D,3D}$ denote the real and imaginary parts of the impedance, respectively.

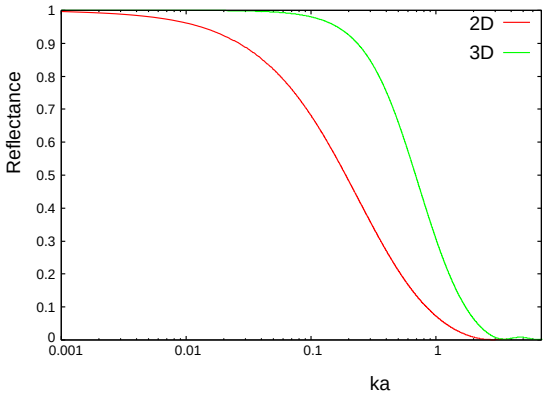

Figure 16: (color online) 2D and 3D reflectances.

and $\mathcal{R} \approx 1 - 2k^2a^2$ for 3D. Fig.16 shows the reflectance of 2D and 3D flanged pipes. While the 3D reflectance starts to decay around $ka = 0.1$, the 2D reflectance decreases around $ka = 0.01$. Then, less sound energy is confined in the 2D pipe by the resonance compared with the 3D pipe. In our 2D model with $a = 2.5$mm, about 83% sound energy is however reflected by the open end even at 1000Hz($ka \approx 0.046$) so that a resonance state is well sustained if its frequency is less than 1000Hz. For the 3D model of the aperture $5 \times 10\text{mm}^2$, the effective radius is estimated as $a \approx 4$mm and about 99% sound energy is reflected by the open end at 1000Hz($ka \approx 0.074$). Note that the 2D reflectance agrees well with the numerical calculation with the

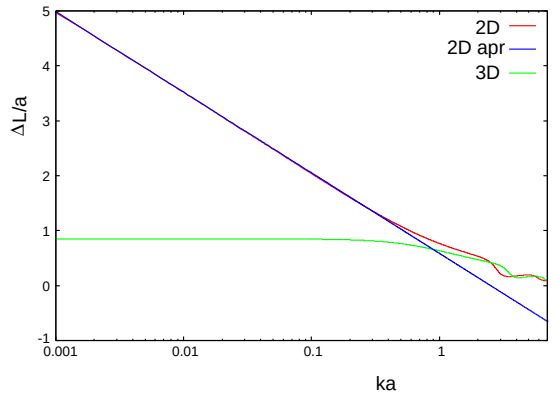

Figure 17: (color online) 2D and 3D end corrections normalized by a together with the approximation for ΔL^{2D} given by eq.(30)(labeled '2D apr').

compressible LES (see refs.[41, 42]).

The end correction of the flanged open end is theoretically given by

$$\Delta L(\omega) = \frac{1}{2k}\arg\left(-\sqrt{R}\frac{Z_R+Z_0}{Z_R-Z_0}\right). \qquad (29)$$

From eqs.(24) and (28), the 2D end correction has an asymptotic form in a low frequency rage as

$$\Delta L^{2D}(\omega) \approx \frac{a}{\pi}(3-2\gamma-2\log ak), \qquad (30)$$

while it becomes $\Delta L^{2D}(\omega) \approx \frac{a}{\pi}(2\log 2\pi+2-2\gamma-2\log ak)$ for the open end pipe without flanges. It diverges logarithmically in the limit of $\omega \to 0$ at least theoretically, while the 3D end correction takes a constant value, $\Delta L^{3D}(\omega) \approx \frac{8a}{3\pi}$. Fig.17 shows the 2D and 3D end corrections calculated with eq.(29) together with the approximation given by eq.(30). The approximation (30) agrees well with the 2D full calculation in the range less than $ka = 0.5$. ΔL^{2D} is larger than ΔL^{3D} in most of the physically relevant range and the difference between them increases as ω goes to zero. Since ΔL^{2D} is estimated as $\Delta L^{2D} \approx 2.5a$ at 1000Hz($ka \approx 0.046$ at $a = 2.5$mm), then $\Delta L^{2D} \approx 6.3$mm, while the 3D model with $\Delta L^{3D} \approx 0.85a$ and with $a \approx 4.0$mm has a correction of $\Delta L^{3D} \approx \frac{8a}{3\pi} \approx 3.4$mm at 1000Hz($ka \approx 0.074$). For a 2D loss-less flanged pipe with a closed remote end, with length of 90mm and with radius of $a = 2.5$mm, the impedance obtained numerically[1] has the first resonance peak at $f_0 = 900$Hz and the second resonance peak(the third harmonic) at $f_1 = 2755$Hz. For a 3D loss-less flanged pipe with the same length and with radius of $a = 4$mm, the impedance has the first resonance peak at 930Hz and the second at 2795Hz.

References

[1] N. H. Fletcher and T. D. Rossing, *The Physics of Musical Instruments*, 2nd Edition (Springer-Verlag, New York 1998).

[2] A. Hirschberg, "Aero-acoustics of Wind instruments" in *Mechanics of Musical Instruments*, Eds. A.Hirschberg, J.Kergomard and G.Weinreich. (Springer-Verlag, Vienna and New York 1995), pp.291-369.

[3] B. Fabre, J. Gilbert, A. Hirschberg and X. Pelorson, "Aeroacoustics of Musical Instruments", Annu. Rev. Fluid Mech. **44** 1-25 (2011).

[4] G. B. Brown, "The vortex motion causing edge tones", Proc. Phys. Soc., London **XLIX** 493-507 (1937).

[5] A. Powell, "On the edgetone", J.Acoust. Soc. Am., **33** 395-409 (1961).

[6] M. S. Howe, *Acoustics of Fluid-Structure Interactions*, (Cambridge Univ. Press, 1998).

[7] D.K. Holger, T.A. Wilson, and Beavers G.S., "Fluid mechanics of the edgetone", J. Acoust. Soc. Am., **62** 1116- 1128 (1977).

[8] D.G. Crighton, "The jet edge-tone feedback cycle; linear theory for the operating stages", J. Fluid Mech., **234** 361-391 (1992).

[9] L. Cremer and H. Ising, "Die selbsterregten Schwingungen von Orgelpfeifen," Acustica **19** 143-153 (1967).

[10] J. W. Coltman, "Sounding mechanism of the flute and organ pipe", J. Acoust. Soc. Am. **44** 983-992 (1968).

[11] J. W. Coltman, "Acoustics of the flute", Physics Today **21** 25-32 (1968).

[12] J. W. Coltman, "Sound Radiation from the Mouth of an Organ Pipe", J. Acoust. Soc. Am. **46** 477 (1969).

[13] J. W. Coltman, "Jet driven mechanisms in edge tones and organ pipes", J. Acoust. Soc. Am. **60** 725-733 (1976).

[14] J. W. Coltman, "Momentum transfer in jet excitation of flute-like instruments", J.Acoust. Soc. Am. **69** 1164-1168 (1981).

[15] N. H. Fletcher and S. Thwaites, "Wave propagation on an acoustically perturbed jet", Acustica **42** 323-334 (1979).

[16] S. Thwaites and N. H. Fletcher, "Wave propagation on turbulent jets", Acustica **45** 175-179 (1980).

[17] S. Thwaites and N. H. Fletcher, "Wave propagation on turbulent jets. II. Growth", Acustica **51** 44-49 (1982).

[18] N. H. Fletcher and S. Thwaites, "The physics of organ pipes", Scientific American **248** 84-93 (1983).

[19] N. H. Fletcher, "Jet-drive mechanism in organ pipes", J. Acoust. Soc. Am. **60** 481-483 (1976).

[20] S. A. Elder, "On the mechanism of sound production on organ pipes", J. Acoust. Soc. Am. **54** 1554-1564 (1973).

[21] S. Yoshikawa and J. Saneyoshi, "Feedback excitation mechanism in organ pipes", J. Acoust. Soc. Jpn. (E) **1** 175-191 (1980).

[22] M. J. Lighthill, "On sound generated aerodynamically. Part I: General theory", Proc. Roy. Soc. London **A211** 564-587 (1952).

[23] N. Curle, "The influence of solid boundaries upon aerodynamics sound", Proc. R. Soc. London **A231** 505-514 (1955).

[24] M.E.Goldstein, *Aeroacoustics*, (McGraw-Hill, 1976).

[25] A. Powell, "Theory of vortex sound", J.Acoust. Soc. Am. **36** 177-195 (1964).

[26] M. S. Howe, "Contributions to the theory of aerodynamic sound with application to excess jet noise an the theory of the flute", J. Fluid Mech. **71** 625-673 (1975).

[27] M. S. Howe, "On the Absorption of Sound by Turbulence and Other Hydrodynamic Flows", IMA J. Appl. Math. **32** 187-209 (1984).

[28] M. P. Verge, B. Fabre, W. E. A. Mahu, A. Hirschberg, R. R. van Hassel, A. P. J. Wijnands, J. J. de Vries, and C. J. Hogendoorn "Jet formation and jet velocity fluctuations in a flue organ pipe", J. Acoust. Soc. Am. **95** 1119-1132 (1994).

[29] M. P. Verge, R. Caussë, B. Fabre, A. Hirschberg, A. P. J. Wijnands, and A. van Steenbergen, "Jet oscillations and jed drive in recorder-like instruments", Acta Acustica **2** 403-419 (1994).

[30] B. Fabre, A. Hirschberg, A. P. J. Wijnands, "Vortex shedding in steady oscillation of a flue organ pipe", Acta Acustica, Acustica **82** 863-877 (1996).

[31] M. P. Verge, B. Fabre, and A. Hirschberg, "Sound production in recorder-like instruments. I. Dimensionless amplitude of the internal acoustic field", J. Acoust. Soc. Am. **101** pp. 2914-2924 (1997).

[32] M. P. Verge, A. Hirschberg, and R. Caussë, "Sound production in recorder-like instruments. II. A simulation model", J. Acoust. Soc. Am. **101** 2925-2939 (1997).

[33] S. Dequand, J. F. H. Willems, M. Leroux, R. Vullings, M. van Weert, C. Thieulot, and A. Hirschberg, "Simplified models of flue instruments: Influence of mouth geometry on the sound source", J. Acoust. Soc. Am. **113** 1724-1735 (2003).

[34] P.A. Skordos, "Modeling flue pipes: subsonic flow, lattice Boltzmann, and parallel Distributed computes", Ph. D. thesis, MIT (1995).

[35] P.A. Skordos, and G.J. Sussman, "Comparison between subsonic flow simulation and physical measurements of flue pipes", Proceedings of

International Symposium on Musical Acoustics 1995, Dourdan, pp.1-6.

[36] H. Kühnelt, “simulating the mechanism of sound generation in flutes using the Lattice boltzmann method”, Proceedings of the Stockholm Music Acoustics Conference 2003, Stockholm, (4pages).

[37] H. Kühnelt, “Simulating and sound generation in flutes and flue pipes with the Lattice-Boltzmann-Method”, Proc. of ISMA 2004, Nara Japan, 251-254.

[38] J. Tsuchida, T. Fujisawa, and G. Yagawa, “Direct numerical simulation of aerodynamic sounds by a compressible CFD scheme with node-by-node finite elements”, Computer Methods in Applied Mechanics and Engineering **195** 1896-1910 (2006).

[39] T. Kobayashi, T. Takami, M. Miyamoto, K. Takahashi, A. Nishida, and M.Aoyagi, “3D Calculation with Compressible LES for Sound Vibration of Ocarina”, Open Source CFD International Conference 2009, November 12-13th, Barcelona, Spain (CD-ROM).

[40] K. Takahashi, M. Miyamoto, Y. Ito, T. Takami, T. Kobayashi, A. Nishida, and M. Aoyagi, “Numerical analysis on 2D and 3D edge tones in terms of aerodynamic sound theory”, Proceedings of International Congress on Acoustics 2010, Sydney (CD-ROM), paper no.621 (8pages).

[41] M. Miyamoto, Y. Ito, K. Takahashi, T. Takami, T. Kobayashi, A. Nishida, and M. Aoyagi, “Applicability of compressible LES to reproduction of sound vibration of an air-reed instrument”, Proceedings of International Symposium on Music Acoustics 2010, Sydney and Katoomba (CD-ROM), paper no.37 (6pages).

[42] K. Takahashi, M. Miyamoto, Y. Ito, T. Takami, T. Kobayashi, A. Nishida, and M. Aoyagi, “Numerical study on air-reed instruments with LES” Proceedings of ASME-JSME-KSME Joint Fluids Engineering Conference 2011, AJK2011-08011 (11pages).

[43] A. Richter, and S. Stefanie Fuß, “Sound production and radiation of resonator-controlled edge tones”, Proceedings of International Congress on Acoustics 2010, Sydney (CD-ROM), paper no.139 (3pages).

[44] S. Fuß, and S. Marburg, “Numerical Computations of a Recorder Fluid”, Proceedings of International Congress on Acoustics 2010, Sydney (CD-ROM), paper no.119 (3pages).

[45] S. Fuß, and S. Marburg, “Numerical Modal Analysis of a Recorder Fluid”, Proceedings of International Symposium on Music Acoustics 2010, Sydney and Katoomba (CD-ROM), paper no.16 (3pages).

[46] S. Yoshikawa, “A pictorial analysis of jet and vortex behaviors during attack transients in organ pipe models”, Acta Acustica, Acustica **86** 623-633 (2000).

[47] C. Ségoufin, B. Fabre, M.P. Verge, A. Hirschberg, and A.P.J.Wijnands, ”Experimental study of the influence of the mouth geometry on sound production in a recorder-like instrument : windway length and chamfers”, Acustica United with Acta Acustica 86 649-661 (2000).

[48] A. Bamberger, “Vortex sound in flutes using flow determination with Endo-PIV”, Forum Acusticum Budapest 2005, 4th European Congress on Acoustics, 665-670 (2005).

[49] A. Bamberger, “Vortex sound of the flue”, Proceedings of ISMA2007, Barcelona Spain, (CD-ROM ISBN:978-84-934142-1-4), 1-S1-5.

[50] J. W. Coltman, “Jet offset, harmonic content, and warble in the flute”, J.Acoust. Soc. Am. **120** 2312-2319 (2006).

[51] E. D. Lauroa, S. D. Martinob, E. Espositoc, M. Falangad, and E. P. Tomasinie “Analogical model for mechanical vibrations in flue organ pipes inferred by independent component analysis”, J. Acoust. Soc. Am. **122** 2413-2424 (2007).

[52] O. Coutier-Delgosha, J. F. Devillers, and A. Chaigne, “Edge-tone instability: Effect of the gas nature and investigation of the feedback

mechanism", Acta. Acust. Acust. **92** 236-246 (2006).

[53] J. Braasch, "Acoustical measurements of expression devices in pipe organs", J. Acoust. Soc. Am. **123** 1683-1693 (2008).

[54] H. J. Auβerlechner, T. Trommer, J. Angster, and A. Miklós "Experimental jet velocity and edge tone investigations on a foot model of an organ pipe," J. Acoust. Soc. Am. **126** 878-886 (2009).

[55] C. Wagner, T. Hüttl, and P. Sagaut, eds. *Large-Eddy Simulation for Acoustics*, (Cambridge Univ. Press, New York, 2007).

[56] P.Oshkai and T.Yan, "Experimental investigation of coaxial side branch resonators" J.Fluids and Structures **24** 589-603 (2008).

[57] S. L. Finnegan, C. Meskell and S. Ziada, "Experimental Investigation of the Acoustic Power Around Two Tandem Cylinders", J. Pressure Vessel Technology **132** 041306 (2010).

[58] L.E. Kinsler, A.R.Frey, A.B. Coppens, and J.V. Sanders, *Fundamentals of Acoustic*, 4th ed. (John Wiley & Sons., 2000).

[59] http://www.openfoam.com/

[60] S. Ghosal, T.S. Lund, P. Moin, and K. Akselvoll, "A dynamic localization model for large-eddy simulation of turbulent flows", J. Fluid Mech., **286** 229-255 (1995).

[61] M. Germano, U. Piomelli, P. Moin, W.H. Cabot, "A dynamic subgrid-scale eddy viscosity model. Physics of fluids a-fluid dynamics", **3**(7) 1760-1765 (1991).

[62] E. Pomraning, and C.J. Rutland, "Dynamic one-equation nonviscosity large-eddy simulation model", AIAA Journal, **40**(4) 689-701 (2002).

[63] D. Bouris, and G. Bergeles, "2D LES of vortex shedding from a square cylinder", Journal of Wind Engineering and Industrial Aerodynamics, **80** 31-46 (1999).

[64] R.H. Kraichnan "Inertial Ranges in Two Dimensional Turbulence", Phys. Fluids **10**, 1417-1423 (1967).

[65] C.E.Leith "Diffusion Approximation for Two Dimensional Turbulence", Phys. Fluids **11**, 671-673 (1968).

[66] G.K.Batchelor, "Computation of the energy spectrum in homogeneous two- dimensional turbulence", Phys. Fluids Suppl. **12** II-233-239 (1969).

[67] T.J. Poinsot, and S. K. Lelef, "Boundary conditions for direct simulations of compressible viscous flows", J. Comp. Phys., **101** 104-129 (1992).

[68] A. W. Nolle, "Sinuous instability of a planar air jet: Propagation parameters and acoustic excitation", J. Acoust. Soc. Am., **103** 3690-3705 (1998).

[69] M.B. Lesser, and J.A. Lewis, "Applications of matched asymptotic expansion methods to acoustics. II. The open-ended duct", J Acoust. Soc. Am., **52** 1406-1410 (1972).